Orbital Angular Momentum-Based Two-Dimensional Super-Resolution Targets Imaging

Authors: Rui Chen[1], Wen-xuan Long[1], Yue Gao[2] and Jiandong Li[1]

[1] State Key Laboratory of Integrated Service Networks
Xidian University, Xian, China

[2] School of EE and CS
Queen Mary University of London, E1 4NS, U.K.

#1114

CONTENTS

INTRODUCTION

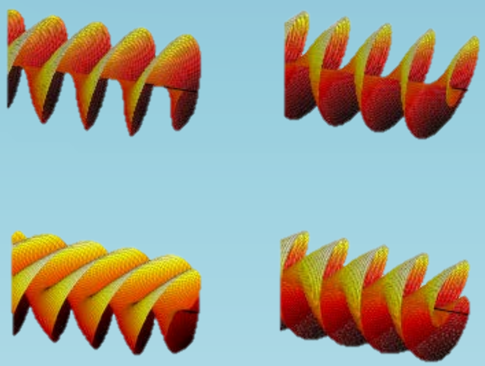

Since the discovery in 1992 that vortex light beams can carry orbital angular momentum (OAM) [1], significant research effort has been focused on the OAM of vortex electromagnetic waves [2], [3] . The phase front of vortex electromagnetic wave rotates with azimuth exhibiting a helical structure $e^{j\alpha\varphi}$ in space as shown in the picture on the left.

Different OAM modes

Inherent orthogonality

A new degree of freedom

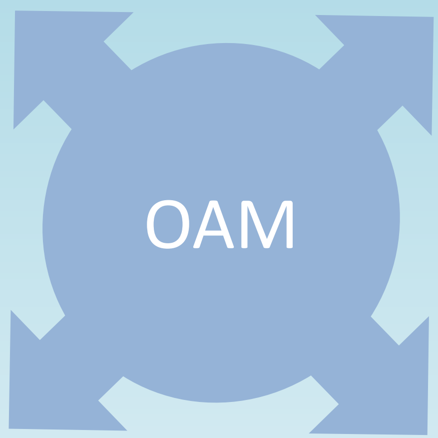

Wireless Communications

Radar

#1114

INTRODUCTION

Radar Application

The helical phase of vortex electromagnetic wave can be seen as multiple plane electromagnetic waves illuminating from continuous azimuth simultaneously

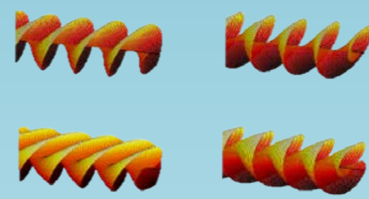

Achieves angular diversity without relative motion or beam scanning

Radar target detection model

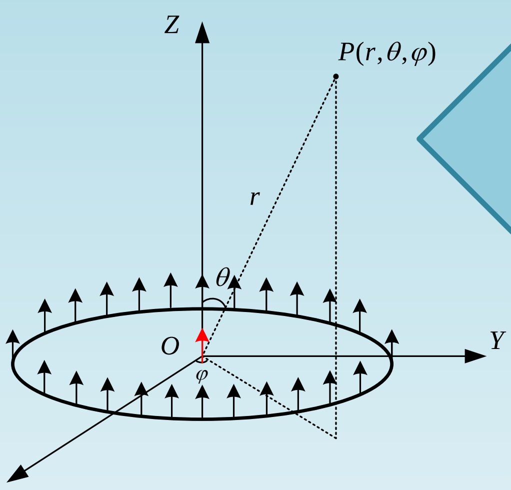

OAM Radar

Azimuth estimation algorithm

Back projection algorithms
FFT algorithms
2-D algorithms
MUSIC algorithm

SYSTEM MODEL

MISO OAM radar targets detection mode

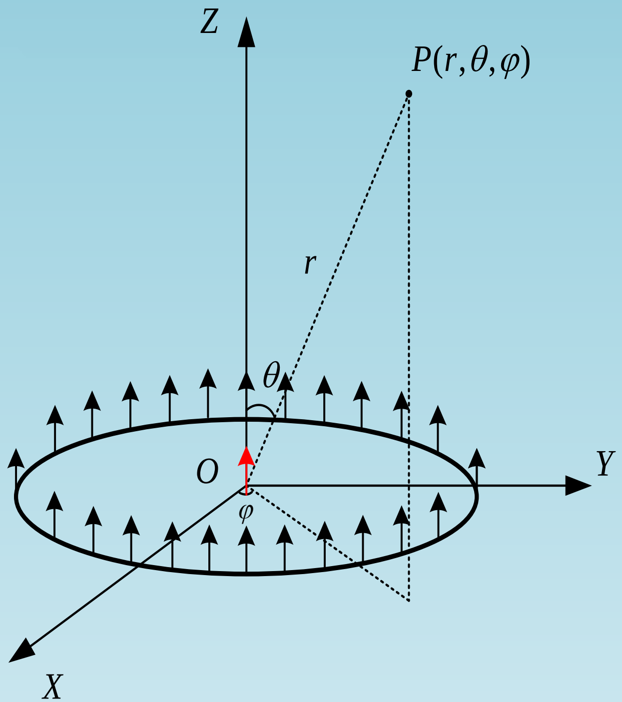

Electric field vector

$$\boldsymbol{E}_s(\boldsymbol{r}) = -\boldsymbol{j}\frac{\mu 0 \omega d N e^{ikr} e^{i\alpha\varphi}}{4\pi r} i^{-\alpha} J_\alpha(kRsin\theta)$$

When $kRsin\theta \gg 1$,

$$J_\alpha(kR\sin\theta) \approx \sqrt{\frac{2}{\pi k a \sin\theta}} \cos\left(kR\sin\theta - \frac{\alpha\pi}{2} - \frac{\pi}{4}\right)$$

Received echo signal

$$s(k,\alpha) = \sum_{m=1}^{M} \sigma'_m e^{i2kr_m} e^{i\alpha\varphi_m} J\alpha(kRsin\theta_m)$$

The N array elements are located uniformly along the perimeter of a circle and are fed with the same input signal but with successive phase shifts $\phi n = \alpha\varphi n = \alpha \cdot \frac{2\pi n}{N}, n = 0, 1, 2, \ldots, N-1$. *Thus, after a full turn the phase has the increment of 2πα .*

#1114

2-D SUPER-RESOLUTION TARGETS IMAGING

Algorism Principle

ESPRIT

Rotational Invariance

- Reduced sensitivity to array perturbations
- Improved performance
- Reduced computational load
- Freedom from array calibration

⟷

2-D super-resolution targets detection based on ESPRIT algorithm

Estimation of Target Range

$$s(k_p) = \sum_{m=1}^{M} \sigma'_m J\alpha(k_p R sin\theta_0) e^{i2kr_m}$$

2-D SUPER-RESOLUTION TARGETS IMAGING

Estimation of Target Range

The echo signal samples

$$\boldsymbol{x}(k) = [\mathrm{s}(k_1)/J_0(k_1 R\sin\theta_0), \mathrm{s}(k_2)/J_0(k_2 R\sin\theta_0), \cdots, \mathrm{s}(k_p)/J_0(k_p R\sin\theta_0)]^{\boldsymbol{T}} = \boldsymbol{A}_r\boldsymbol{\sigma} + \mathbf{n}$$

The covariance matrix

$$\boldsymbol{R}_x = \mathbf{E}[\boldsymbol{x}(k)\boldsymbol{x}^{\boldsymbol{H}}(k)] = \boldsymbol{A}_r\boldsymbol{R}_\sigma\mathbf{A}_r^{\boldsymbol{H}} + \boldsymbol{\rho}_n\boldsymbol{\Lambda}_J$$

Where

$$\boldsymbol{A}_r = \begin{matrix} e^{i2k1r1} & e^{i2k1r2} & \cdots & e^{i2k1r\mathrm{M}} \\ e^{i2k2r1} & e^{i2k2r2} & \cdots & e^{i2k2r\mathrm{M}} \\ \vdots & \vdots & \ddots & \vdots \\ e^{i2k\mathrm{P}r1} & e^{i2k\mathrm{P}r2} & \cdots & e^{i2k\mathrm{P}r\mathrm{M}} \end{matrix}$$

$$\boldsymbol{\sigma} = [\sigma_1', \sigma_2', \cdots, \sigma_M']^T$$

$$\boldsymbol{n} = [n_1/J_0(k_1 R\sin\theta_0), n_2/J_0(k_2 R\sin\theta_0), \cdots, n_P/J_0(k_P R\sin\theta_0)]^T$$

$$\boldsymbol{\Lambda}_J = diag\{J_0^{-2}(k_1 R\sin\theta_0), J_0^{-2}(k_2 R\sin\theta_0), \cdots, J_0^{-2}(k_P R\sin\theta_0)\}$$

$$\boldsymbol{R}_\sigma = \mathbf{E}[\boldsymbol{\sigma}\boldsymbol{\sigma}^H]$$

2-D SUPER-RESOLUTION TARGETS IMAGING

Estimation of Target Range

Singular Value Decomposition (SVD) Algorithm

Eigenvalue Decomposition:

$$\mathbf{R}_X = \boldsymbol{Q}\boldsymbol{\Lambda}\boldsymbol{Q}^H$$

Where

$$\boldsymbol{\Lambda} = diag\{\lambda_1, \lambda_2, \cdots, \lambda_M\}$$

Eigenvalue Decomposition:

$$\mathbf{R}_X\boldsymbol{q} = \lambda_{max}\boldsymbol{q}$$

Where

$$\boldsymbol{q} = [\mathrm{q}_1, \mathrm{q}_2, \cdots, \mathrm{q}_P]^{\mathrm{T}}$$

Reconstruct the Covariance Matrix

$$\boldsymbol{R}^f = \begin{matrix} \mathrm{q}_1 & \mathrm{q}_2 & \mathrm{q}_3 & \cdots & \mathrm{q}_{P-i+1} \\ \mathrm{q}_2 & \mathrm{q}_3 & \mathrm{q}_4 & \cdots & \mathrm{q}_{P-i+2} \\ \mathrm{q}_3 & \mathrm{q}_4 & \mathrm{q}_5 & \cdots & \mathrm{q}_{P-i+3} \\ \vdots & \vdots & \vdots & \ddots & \vdots \\ \mathrm{q}_i & \mathrm{q}_{i+1} & \mathrm{q}_{i+2} & \cdots & \mathrm{q}_P \end{matrix}$$

2-D SUPER-RESOLUTION TARGETS IMAGING

Estimation of Target Range

The steps of target range estimation

(i) Calculate the eigenvector $\boldsymbol{q}$ corresponding to the largest eigenvalue of the covariance matrix $\mathbf{R}_{\boldsymbol{X}}$.

(ii) Reeconstruct $\boldsymbol{R}^{f}$ based on $\boldsymbol{q}$.

(iii) Perform SVD on $\mathbf{R}^{f}$ as $\mathbf{R}^{f} = \widehat{\boldsymbol{U}}\sum\widehat{\boldsymbol{V}}^{\boldsymbol{H}}$

Where $\widehat{\boldsymbol{U}}$ is an $\boldsymbol{i} \times \boldsymbol{i}$ unitary matrix and $\widehat{\boldsymbol{V}}$ is a $(\boldsymbol{P}-\boldsymbol{i}+\mathbf{1}) \times (\boldsymbol{P}-\boldsymbol{i}+\mathbf{1})$ unitary matrix. Then, we can obtain signal subspace $\widehat{\boldsymbol{U}}_{\boldsymbol{s}}$ that is the part of $\widehat{\boldsymbol{U}}$ corresponding to M large singular values containing distance information of M targets.

(iv) Construct new matrices $\widehat{\boldsymbol{U}}_{\mathbf{1}}$ taking the first $\boldsymbol{i}-\mathbf{1}$ rows of $\widehat{\boldsymbol{U}}_{\boldsymbol{s}}$ and $\widehat{\boldsymbol{U}}_{\mathbf{2}}$ taking the last $\boldsymbol{i}-\mathbf{1}$ rows of $\widehat{\boldsymbol{U}}_{\boldsymbol{s}}$.

(v) Calculate $\boldsymbol{\Psi} = (\widehat{\boldsymbol{U}}_1^{\mathrm{H}}\widehat{\mathbf{U}}_{\mathbf{1}})^{-1}\widehat{\boldsymbol{U}}_1^{\mathrm{H}}\widehat{\mathbf{U}}_{\mathbf{2}}$

(vi) Perform eigenvalue decomposition on $\boldsymbol{\Psi}$ as $\boldsymbol{\Psi} = \widehat{\boldsymbol{Q}}\boldsymbol{\Lambda}_{\boldsymbol{r}}\widehat{\boldsymbol{Q}}^{-\mathbf{1}}$.

Where $\boldsymbol{\Lambda}_{\boldsymbol{r}} = \mathrm{diag}\{e^{i2r1}, e^{i2r2}, \cdots, e^{i2r\mathrm{M}}\}$

#1114

Estimation of Target Azimuth

The echo signal samples

$$\boldsymbol{y}(\alpha) = [\mathrm{s}(\alpha_1)/J_{\alpha_1}(k_p R\sin\theta_0), \mathrm{s}(\alpha_2)/J_{\alpha_2}(k_p R\sin\theta_0), \cdots, \mathrm{s}(\alpha_Q)/J_Q(k_p R\sin\theta_0)]^{\boldsymbol{T}} = \boldsymbol{A}_\varphi \boldsymbol{a} + \mathbf{m}$$

Where

$$\boldsymbol{A}_\varphi = \begin{matrix} e^{i\alpha 1\varphi 1} & e^{i\alpha 1\varphi 2} & \cdots & e^{i\alpha 1\varphi \mathrm{M}} \\ e^{i\alpha 2\varphi 1} & e^{i\alpha 2\varphi 2} & \cdots & e^{i\alpha 2\varphi \mathrm{M}} \\ \vdots & \vdots & \ddots & \vdots \\ e^{i\alpha \mathrm{Q}\varphi 1} & e^{i\alpha \mathrm{Q}\varphi 2} & \cdots & e^{i\alpha \mathrm{Q}\varphi \mathrm{M}} \end{matrix}$$

$$\boldsymbol{a} = [a_1(k_p), a_2(k_p), \cdots, a_M(k_p)]^{\mathbf{T}},\ a_m(k_p) = \sigma_m' e^{i2k_p r_m} J_\alpha(k_p R sin\theta_m)$$

2-D SUPER-RESOLUTION TARGETS IMAGING

Numerical Simulation and Results

Simulation Data

$r_1 = 40m, r_2 = 45m, r_3 = 50m$

$(\varphi_1, \theta_1) = (10°, 70°), (\varphi_2, \theta_2) = (15°, 70°), (\varphi_3, \theta_3) = (20°, 70°)$

Discrete frequencies: 9.024GHz to 9.979GHz

Wave number： $k = 189, 190, \cdots, 209$

OAM modes: $\alpha = -16, -15, \cdots, 15$

2-D SUPER-RESOLUTION TARGETS IMAGING

Numerical Simulation and Results

Simulation Result

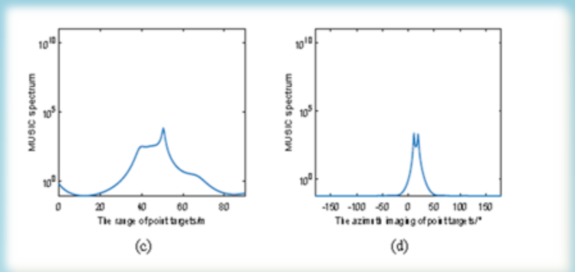

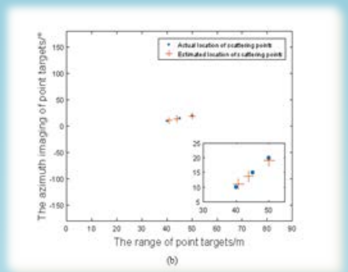

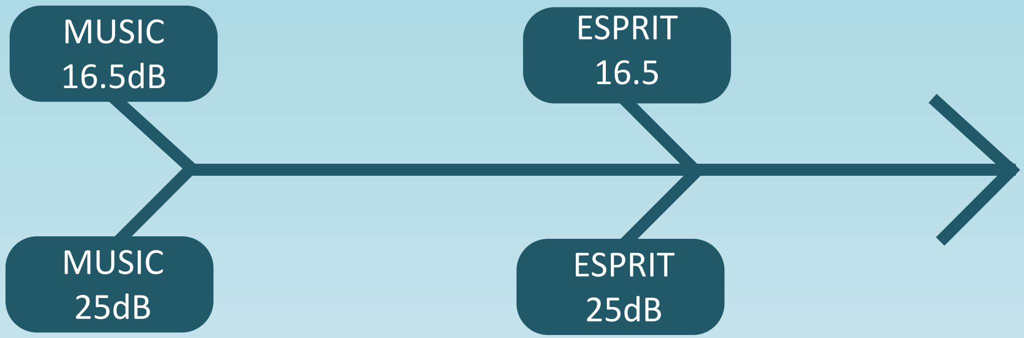

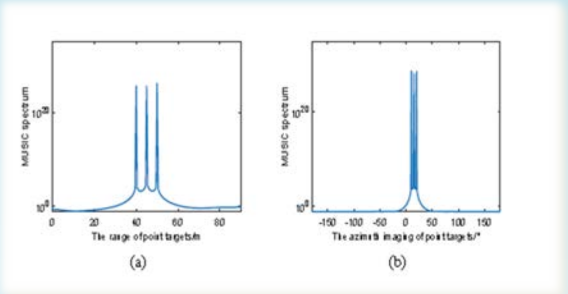

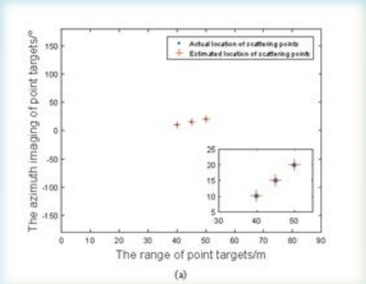

Both MUSIC and ESPRIT algorithms-based methods can fulfill 2-D imaging of three close point targets at higher SNR, however, ESPRIT algorithms-based methods can provide the positions of targets directly instead of searching spectrum peaks. Furthermore, at lower SNR ESPRIT method can still distinguish three point targets while only one or two blunt peaks could be seen by MUSIC method. It follows that the proposed ESPRIT algorithm-based method is more robust to the MUSIC algorithm-based method.

#1114

CONCLUSIONS

ESPRIT algorithm-based 2-D OAM radar targets detection method shows the 2-D super-resolution capability of OAM-based radar. In contrast to conventional algorithm, both MUSIC algorithm-based radar targets detection and ESPRIT algorithm-based OAM radar targets detection belong to super-resolution imaging methods. Meanwhile, our proposed ESPRIT algorithm-based 2-D OAM radar targets detection method further outperforms MUSIC.

THANKS!

#1114

References

[1] L. Allen, M. W. Beijersbergen, R. Spreeuw, and et al., “Orbital angular momentum of light and the transformation of laguerre-gaussian laser modes,” Phys. Rev. A, vol. 45, no. 11, pp. 8185–8189, Jul. 1992.
[2] F. Tamburini, E. Mari, A. Sponselli, and et al., “Encoding many channels on the same frequency through radio vorticity: First experimental test,” New J. Phy., vol. 14, no. 3, p. 033001, Mar. 2012.
[3] S. M. Mohammadi, L. K. Daldorff, J. E. Bergman, and et al., “Orbital angular momentum in radioła system study,” IEEE Trans. Antenn. Propag., vol. 58, no. 2, pp. 565–572, Feb. 2010.
[4] Y. Yan and et al., “High-capacity millimetre-wave communications with orbital angular momentum multiplexing,” Nat. Commun., vol. 5, no. 4876, p. 4876, Sept. 2014.
[5] R. Gaffoglio, A. Cagliero, A. D. Vita, and B. Sacco, “OAM multiple transmission using uniform circular arrays: Numerical modeling and experimental verification with two digital television signals,” Radio Sci., vol. 51, no. 6, pp. 645–658, Jun. 2016.
[6] G. R. Guo, W. D. Hu, and X. Y. Du, “Electromagenetic vortex based radar target imaging (in chinese),” J. Nat. Univ. Defense Technol., vol. 35, no. 6, pp. 71–76, Dec. 2013.
[7] K. Liu, Y. Cheng, Z. Yang, H. Wang, Y. Qin, and X. Li, “Orbitalangular-momentum-based electromagnetic vortex imaging,” IEEE Antennas Wirel. Propag. Lett., vol. 14, pp. 711–714, Dec. 2015.

References

[8] M. Lin, Y. Gao, P. Liu, and et al., “Super-resolution orbital angular momentum based radar targets detection,” Electron. Lett., vol. 52, no. 13, pp. 1168–1170, Jun. 2016.

[9] ——, “Improved OAM-based radar targets detection using uniform concentric circular arrays,” Int. J. Antenn. Propag., vol. 2016, no. 6, pp. 1–8, Jan. 2016.

[10] B. Thid´e, H. Then, J. Sj¨oholm, and et al., “Utilization of photon orbital angular momentum in the low-frequency radio domain,” Phys. Rev. Lett., vol. 99, no. 8, p. 087701, Aug. 2007.

[11] F. E. Mahmouli and S. Walker, “Orbital angular momentum generation in a 60ghz wireless radio channel,” in Proc. 20th IEEE TELFOR, Nov. 2012, pp. 315–318.

[12] R. Roy and T. Kailath, “ESPRIT-estimation of signal parameters via rotational invariance techniques,” IEEE Trans. Acoust. Speech & Signal Process., vol. 37, no. 7, pp. 984–995, Jul. 1989.

[13] Y. Wang, H. Chen, Y. Peng, and et al., Theory and algorithms of spatial spectrum estimation. Tsinghua University Press, 2004, ch. Multiple signal classification method, pp. 106–107.